RSC Advances

PAPER

View Article Online
View Journal | View Issue

Cite this: *RSC Adv.*, 2024, **14**, 33061

Ascorbic acid mediated fluorescence emission of MnO_2 modified upconversion nanoparticles for anti-counterfeiting

Yongling Zhang, *[ab] Xiang Liu,[b] Yuhai Wang,[b] Mingxing Song[b] and Zhengkun Qin *[b]

Anti-counterfeiting ink can prevent important documents from being forged or tampered with. We reported a strategy to improve upconversion luminescence intensity of $NaYF_4$:18%Yb^{3+},0.5%Tm^{3+} core nanoparticles (NPs) by coating the $NaYF_4$ shell. We synthesized $NaYF_4$:18%Yb^{3+},0.5%Tm^{3+} core NPs and $NaYF_4$:18%Yb^{3+},0.5%Tm^{3+}/$NaYF_4$ core–shell NPs by high temperature thermal decomposition method. In comparison with the core NPs, the upconversion luminescence intensity of the core–shell NPs was enhanced by 2.3 times in the wavelength range of 445 nm to 495 nm. We designed composite nanomaterials based on $NaYF_4$:Yb^{3+},Tm^{3+}/$NaYF_4$ core–shell NPs and MnO_2, and synthesized $NaYF_4$:Yb^{3+},Tm^{3+}/$NaYF_4$@MnO_2 composite NPs by physical doping method. Here, MnO_2 acts as a quencher to quench the upconversion fluorescence of Tm^{3+} ions of the core–shell NPs. Afterwards, we used the prepared product for document anti-counterfeiting. And then reducing agent (AA) can destroy the structure of MnO_2 to restore the upconversion luminescence of Tm^{3+} ions. We use $NaYF_4$:18%Yb^{3+},0.5%Tm^{3+}/$NaYF_4$@MnO_2 composite NPs as anti-counterfeiting ink to write the letter "L". Under ambient conditions or the irradiation of 980 nm continuous light, "L" does not emit light. After AA is evenly applied on the letter "L", "L" can emit blue fluorescence under the irradiation of 980 nm continuous light. These results showed that $NaYF_4$:Yb^{3+},Tm^{3+}/$NaYF_4$@MnO_2 composite NPs can be used in important document anti-counterfeiting tasks to enhance information security.

Received 16th August 2024
Accepted 20th September 2024

DOI: 10.1039/d4ra05938g

rsc.li/rsc-advances

1. Introduction

Important documents may be forged and tampered with by malicious individuals during the transmission process. For example, key statements and signatures in commercial documents are forged and tampered with by malicious individuals, leading to legal disputes.[1–3] Therefore, it is very necessary to create a safe, effective and easy to popularize anti-counterfeiting technique. Among many anti-counterfeiting techniques, luminescent materials are undoubtedly the best choice because of their unique physico-chemical and optical properties, which can make complex patterns printed on different substrates.[4–7] Rare-earth upconversion luminescent materials are often chosen; they can enable conversion from near-infrared light to visible light due to the anti-stokes effect where two or more low-energy photons are sequentially absorbed, and then higher-energy photons are emitted.[8–11] Rare-earth upconversion luminescent materials have the characteristics of strong photostability, long fluorescence lifetime, simple synthesis method and low toxicity and stable chemical properties, which allow us to effectively use them in anti-counterfeiting work.[12–15] Over the past few decades, anti-counterfeiting technology based on rare-earth upconversion luminescent materials has been researched and applied by researchers in different degrees.[16–19] Mengxiao Li's team[20] proposed to coat a layer of novel fluorescent carbon quantum dots (CDs) on the surface of the synthesized $NaYF_4$:RE^{3+} nanomaterials and mixed them with poly (acrylic acid) (PAA) aqueous solution as an anti-counterfeiting ink. They used the anti-counterfeiting ink to print out QR codes, clover and other patterns. These patterns can't be seen under visible light irradiation. But blue fluorescence patterns can be observed under 365 nm UV light irradiation, and green fluorescence patterns can be observed under 980 nm continuous pump light irradiation, so the material can be used in anti-counterfeiting technology. Wu Wei *et al.*[21] choose traditional screen printing technology to deposit water-soluble $NaYF_4$:Yb^{3+},Tm^{3+}/Er^{3+}/Eu^{3+} upconversion NPs on paper and polyethylene terephthalate(PET) and made different patterns. There was no pattern on paper. There were white patterns on PET. Under 980 nm continuous pump light irradiation, the blue, yellow-green and green fluorescence corresponding to $NaYF_4$:Yb^{3+},Tm^{3+}/Er^{3+}/Eu^{3+} upconversion NPs can be observed on

[a]School of Chemistry and Pharmaceutical Engineering, Jilin Institute of Chemical Technology, Jilin 132022, China. E-mail: yong1ling@163.com
[b]College of Information & Technology, Jilin Normal University, Siping 136000, China. E-mail: qin_zhengkun@126.com

paper and PET, respectively. Huang Ling *et al.*[22] prepared $NaYF_4$:2%Er^{3+},0.5%Tm^{3+}/$NaYF_4$ core–shell NPs by high temperature thermal decomposition method, and made them as anti-counterfeiting ink to write the letters "I, A, M". Under 980 nm continuous pump light irradiation and the repetition rate was constant at 100 Hz, the letters "I, A, M" emitted green upconversion fluorescence when the pulse time was 100 us; the letters "I, A, M" emitted yellow upconversion fluorescence when the pulse time was 500 μs; the letters "I, A, M" emitted red upconversion fluorescence when the pulse time was 6000 us. But these anti-counterfeiting technologies are single and easy to crack, so we have been studying a more precise anti-counterfeiting technology, so that the anti-counterfeiting security is stronger.

In this article, we proposed to wrap a $NaYF_4$ passive shell outside $NaYF_4$:18%Yb^{3+},0.5%Tm^{3+} core NPs to improve the luminescence intensity of $NaYF_4$:18%Yb^{3+},0.5%Tm^{3+}/$NaYF_4$ core–shell NPs. The upconversion luminescence intensity (~477 nm) of the NPs was enhanced by 2.3 times after coating a $NaYF_4$ passive shell, due to the surface luminescence quenching effect was suppressed by wrapping the passive shell. Then we physically mixed high-luminosity core–shell NPs with MnO_2 nanosheets to form $NaYF_4$:18%Yb^{3+},0.5%Tm^{3+}/$NaYF_4$@MnO_2 composite NPs. We found resonant energy transfer between MnO_2 and Tm^{3+} ions can quench the upconversion luminescence of core–shell NPs. We also found that AA can disrupt the structure of MnO_2 and reduce it to Mn^{2+} ions, and that Mn^{2+} ions can't occur energy transfer with Tm^{3+} ions, thus restoring the upconversion luminescence of the core–shell NPs. Finally, we conducted the experiments about composite NPs on anti-counterfeiting research and concluded that they can further enhance the security of anti-counterfeiting.

2. Experimental

2.1 Chemicals

Yttrium acetate hexahydrate($Y(CH_3COO)_3\cdot 6H_2O$), Ytterbium acetate hexahydrate($Yb(CH_3COO)_3\cdot 6H_2O$) and Thulium acetate hexahydrate($Tm(CH_3COO)_3\cdot 6H_2O$) were purchased from Jining Tianyi New Materials Co., Ltd, Shandong, China. Oleic acid (OA), 1-octadecene (ODE) and ammonium fluoride (NH_4F) were purchased from Alfa Aesar Co., Ltd, Shanghai, China. Sodium hydroxide was purchased from Tianjin Guangfu Techology Development Co., Ltd, China. Potassium hypermanganate ($KMnO_4$) was purchased from Tianjin Fuchen Reagent Co., Ltd, China. Methanol (CH_3OH) and ethanol (CH_3CH_2OH) were purchased from Sinopharm Chemical Reagents Co., Ltd, China. Cyclohexane (C_6H_{12}) was purchased from Chengdu Cologne Chemical Co., Ltd, China.

2.2 Synthetic procedures

2.2.1 Preparation of $NaYF_4$:18%Yb^{3+},0.5%Tm^{3+} core NPs.[23] 0.326 mmol of $Y(CH_3COO)_3\cdot 6H_2O$, 0.072 mmol of $Yb(CH_3COO)_3\cdot 6H_2O$, 0.002 of mmol $Tm(CH_3COO)_3\cdot 6H_2O$, 4 mL of OA, and 6 mL of ODE were placed into a 50 mL two-neck flask. Under the protection of argon flow, the temperature of the reaction solution was raised to 150 °C and stirred for 1 hour. Next, the reaction solution temperature was cooled to room temperature naturally. 0.04 g of NaOH and 0.04884 g of NH_4F were dissolved in 8 mL of methanol by ultrasound. Then, the methanol solutions of NaOH and NH_4F were added to the two-neck flask and stirred for 30 min. After that, the reaction system was raised to 60 °C and stirred for 0.5 hours to remove the methanol. The reaction solution was raised to 300 °C and kept for 1 hour under the protection of argon gas. Finally, the reaction system was cooled to room temperature and washed with cyclohexane and ethanol for four times. The final product was dispersed in 4 mL cyclohexane solution.

2.2.2 Preparation of $NaYF_4$:18%Yb^{3+},0.5%Tm^{3+}/$NaYF_4$ core–shell NPs.[24,25] 0.4 mmol of $Y(CH_3COO)_3\cdot 6H_2O$, 4 mL of OA and 6 mL of ODE were placed in a 50 mL two-neck flask. Next, the reaction solution was raised to 150 °C and stirred for 1 hour under argon gas protection. The reaction solution was cooled to room temperature naturally. After, 4 mL of cyclohexane solution containing 0.4 mmol $NaYF_4$:Yb^{3+},Tm^{3+} core NPs was added to the reaction system. 0.04 g NaOH and 0.04884 g NH_4F were added to 8 mL methanol solution until completely dissolved. Then, the mixed solution is added dropwise to the reaction system. After that, the reaction solution was raised to 60 °C and stirred for 1 hour to remove methanol. Subsequently, the reaction solution was raised to 300 °C and kept for 1 h. Finally, the reaction solution was cooled to room temperature and washed with cyclohexane and ethanol for four times, the final product was dispersed in 4 mL ethanol solution, the core–shell NPs solution. The concentration of the core–shell NPs solution is 1 mol L^{-1}.

2.2.3 Preparation of MnO_2 nanosheets.[26] 0.1 mmol of $KMnO_4$ was dissolved in 40 mL deionized water and stirred for 10 min, continuously. After the solution was poured into a 50 mL Teflon-lined autoclave. Then, the reaction system heated to 160 °C and kept for 2 hours. After, the reaction system was cooled to room temperature, the product was washed three times with deionized water and ethanol. Finally, the product was dissolved in 5 mL of deionized water to form MnO_2 solution with a concentration of 0.01 mol L^{-1}.

2.2.4 Preparation of NPs@MnO_2 composite NPs. 0.08 mL of ethanol solution containing $NaYF_4$:Yb^{3+},Tm^{3+}/$NaYF_4$ core–shell NPs (0.008 mmol) was added to 15 mL of deionized water containing MnO_2 solution (0.012 mmol), At room temperature. The mixed solution was stirred for 20 minutes to synthesize the core–shell NPs@MnO_2 composite NPs. Finally, the sample was washed with deionized water and ethanol. The sample was dispersed in 1 mL deionized water.

2.3 Characterization

The crystal phase of the samples were measured by Model Rigaku Ru-200b X-ray powder analyzer produced by Rigaku Corporation Japan (λ = 1.5406 Å, scanning range from 10° to 70°). Morphological of products were measured by a High Resolution Transmission Electron Microscope (JEM-F200). Upconversion fluorescence spectra of these products were measured by a Hitachi F-4500 fluorescence spectrometer. Anti-counterfeiting application photos were taken by Nikon D3200.

3. Results and discussion

$NaYF_4$:18%Yb^{3+},0.5%Tm^{3+} core NPs was prepared by high-temperature thermal decomposition method. And further $NaYF_4$:18%Yb^{3+},0.5%Tm^{3+}/$NaYF_4$ core–shell NPs was prepared by a coating $NaYF_4$ shell method. The XRD standard card of β-phase $NaYF_4$ (JCPDS: 16-334) is shown in Fig. 1(a). The crystal phase of the samples was tested by using X-ray diffraction (XRD), as shown in Fig. 1(b) and (c). We can see that all diffraction peaks of the prepared samples can match well with the $NaYF_4$ standard PDF (JCPDS: 16-334) without any other impurity peaks, exhibiting a β-phase structure, confirming that the coating of a $NaYF_4$ passive shell has no effect on crystal phase of the sample. Transmission Electron Microscope (TEM) images of $NaYF_4$:18%Yb^{3+},0.5%Tm^{3+} core NPs and $NaYF_4$:18%Yb^{3+},0.5%Tm^{3+}/$NaYF_4$ core–shell NP. The TEM image of as-prepared $NaYF_4$:Yb^{3+},Tm^{3+} core NPs and as-prepared $NaYF_4$:Yb^{3+},Tm^{3+}/$NaYF_4$ core–shell NPs are presented in Fig. 1(b) and (c). As can be seen from Fig. 1(b), that the shapes of $NaYF_4$:Yb^{3+},Tm^{3+} core NPs is hexagonal and have uniform morphology. The average size of the as-prepared core NPs is about 140 nm. From Fig. 1(c), it can be seen that the $NaYF_4$:Yb^{3+},Tm^{3+}/$NaYF_4$ core–shell NPs is also hexagonal and the average size of the as-prepared core–shell NPs is about 190 nm. The above results indicate that after coating $NaYF_4$ shell, the morphology of the as-prepared NPs did not change, and the average size of the as-prepared core–shell NPs increased, with the $NaYF_4$ shell thickness of about 50 nm.

Fig. 2(a) is schematic structure diagram of $NaYF_4$:Yb^{3+},Tm^{3+} core NPs and $NaYF_4$:Yb^{3+},Tm^{3+}/$NaYF_4$ core–shell NPs. To explore the effect of $NaYF_4$ shell on the luminescence properties of the as-prepared sample, we tested the upconversion fluorescence spectra of $NaYF_4$:18%Yb^{3+},0.5%Tm^{3+} core NPs and $NaYF_4$:18%Yb^{3+},0.5%Tm^{3+}/$NaYF_4$ core–shell NPs under 980 nm continuous light excitation. The test results are shown in the figure Fig. 2(b). From the upconversion emission spectra, there are five emission peaks can be observed at 345 nm, 363 nm, 451 nm, 477 nm and 644 nm, which correspond to the radiative transitions of Tm^{3+} ions: $^1I_6 \rightarrow {}^3F_4$, $^1D_2 \rightarrow {}^3H_6$, $^1D_2 \rightarrow {}^3F_4$, $^1G_4 \rightarrow {}^3H_6$ and $^3F_3 \rightarrow {}^3H_6$. From Fig. 2(b), we can also see that the upconversion luminescence intensity of $NaYF_4$ core NPs is relatively weak. This is because the core NPs have a larger specific surface area and more surface defects, which will lead to the occurrence of surface luminescence quenching effect. After coating with the $NaYF_4$ shell, the upconversion emission intensity of the NPs was significantly enhanced under the excitation of 980 nm continuous light, as shown in Fig. 2(b). Fig. 2(c) shows the ratio of the luminescence intensity of the upconversion emission peaks of the core NPs and the core–shell NPs under 980 nm continuous pump light excitation. After coating a $NaYF_4$ shell on the core NP, its upconversion luminescence intensity (~477 nm) is 2.3 times that of the core NPs, due to the surface passivation,[27] as shown in Fig. 2(c). The above results indicate that coating a $NaYF_4$ shell on the core NPs can effectively enhance its upconversion luminescence intensity. Therefore, a high brightness core–shell NP with a size of approximately 190 nm was prepared using core–shell coating method and used for subsequent research. In addition, we also tested the fluorescence attenuation curve the fluorescence decay curve of $^1G_4$ energy level of Tm^{3+} of $NaYF_4$:Yb^{3+},Tm^{3+} core NPs and $NaYF_4$:Yb^{3+},Tm^{3+}/$NaYF_4$ core–shell NPs, as shown in Fig. 2(d) and (e). After being coated with a $NaYF_4$ shell, lifetimes

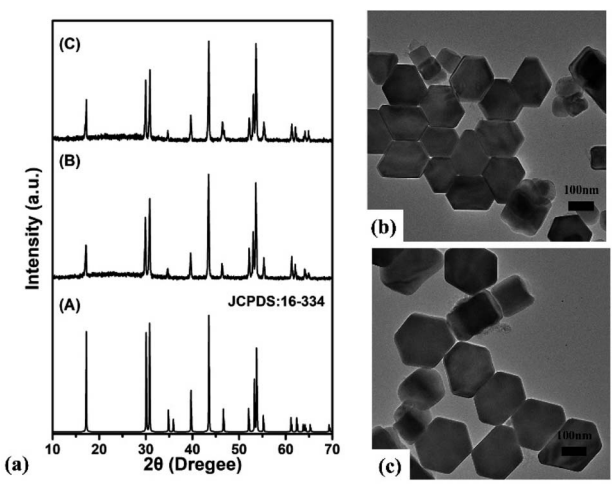

Fig. 1 (a) XRD patterns of (A) β-phase standard card $NaYF_4$ (JCPDS: 16-334), (B) $NaYF_4$:18%Yb^{3+},0.5%Tm^{3+} core NPs, (C) $NaYF_4$:18%Yb^{3+},0.5%Tm^{3+}/$NaYF_4$ core–shell NPs. (b) The TEM images of $NaYF_4$:18%Yb^{3+},0.5%Tm^{3+} core NPs. (c) The TEM images of $NaYF_4$:18%Yb^{3+},0.5%Tm^{3+}/$NaYF_4$ core–shell NPs.

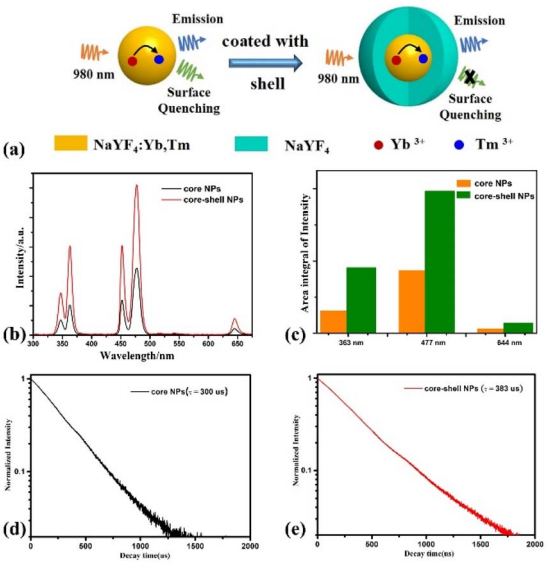

Fig. 2 (a) Schematic structure diagram of $NaYF_4$:18%Yb^{3+},0.5%Tm^{3+} core NPs and $NaYF_4$:18%Yb^{3+},0.5%Tm^{3+}/$NaYF_4$ core–shell NPs. (b) Upconversion emission spectra of $NaYF_4$:18%Yb^{3+},0.5%Tm^{3+} core NPs and $NaYF_4$:18%Yb^{3+},0.5%Tm^{3+}/$NaYF_4$ core–shell NPs under the excitation of 980 nm continuous pump light. (c) The ratio of the luminescence intensity of the upconversion emission peaks of the core NPs and the core–shell NPs under 980 nm continuous pump light excitation. The fluorescence decay curve of $^1G_4$ energy level of Tm^{3+} of (d) the core NPs and (e) the core–shell NPs.

of $^1G_4$ energy level of Tm^{3+} of the $NaYF_4$:Yb^{3+},Tm^{3+} core NPs increased from 300 μs to 383 μs. This is because the shell coating can effectively reduce the surface defects of the NPs. The lifetime variation trend and fluorescence spectral intensity variation trend of the core NPs and the core–shell NPs are consistent, as shown in Fig. 2(b).

$NaYF_4$:18%Yb^{3+},0.5%Tm^{3+}/$NaYF_4$ core–shell NPs was prepared by high-temperature thermal decomposition method. MnO_2 nanosheets was synthesized by hydrothermal method, and $NaYF_4$:18%Yb^{3+},0.5%Tm^{3+}/$NaYF_4$@MnO_2 composite NPs was synthesized by physical mixing method. We measured the XRD of these samples. The XRD standard card of β-phase $NaYF_4$ (JCPDS: 16-334), $NaYF_4$:Yb^{3+},Tm^{3+}/$NaYF_4$ core–shell NPs, the XRD standard card of δ-phase MnO_2 (JCPDS: 80-1098), MnO_2 nanosheets and $NaYF_4$:Yb^{3+},Tm^{3+}/$NaYF_4$@MnO_2 composite NPs was displayed in Fig. 3(a). From Fig. 3(a), it can be observed that the diffraction peaks of as-prepared core–shell NPs is sufficient to match that of β-phase $NaYF_4$, and the diffraction peaks of as-prepared MnO_2 nanosheets can be matched well with pure δ-phase MnO_2. We can observe the crystal phase of as-prepared the core–shell NPs is β-phase $NaYF_4$, and the crystal phase of MnO_2 nanosheets is δ-phase MnO_2. The composite NPs have all the diffraction peaks of the δ-phase MnO_2 and the β-phase $NaYF_4$, which indicates that we have successfully prepared $NaYF_4$:Yb^{3+},Tm^{3+}/$NaYF_4$@MnO_2 composite NPs. Fig. 2(b) is the TEM image of MnO_2 nanosheets, whose shape is in a flower-like nanosheet. The prepared δ-phase MnO_2 nanosheets have a birnessite framework and layered structure, whose layered thickness is about ∼35 nm. Fig. 2(c) is the TEM image of $NaYF_4$:Yb^{3+},Tm^{3+}/$NaYF_4$@MnO_2 composite NPs. It can be observed that the MnO_2 nanosheets are evenly mixed with $NaYF_4$:Yb^{3+},Tm^{3+}/$NaYF_4$ core–shell NPs to form composite NPs.

To investigate the effect of MnO_2 nanosheets on the luminescence properties of $NaYF_4$:Yb^{3+},Tm^{3+}/$NaYF_4$ core–shell NPs, we tested the upconverted luminescence spectra of $NaYF_4$:Yb^{3+},Tm^{3+}/$NaYF_4$ core–shell NPs and $NaYF_4$:Yb^{3+},Tm^{3+}/$NaYF_4$@MnO_2 composite NPs under 980 nm continuous pump light excitation. A in Fig. 4(a) is the upconversion luminescence spectra of $NaYF_4$:Yb^{3+},Tm^{3+}/$NaYF_4$/$NaYF_4$ core–shell NPs. Under 980 nm continuous pump light excitation, we can see $NaYF_4$:Yb^{3+},Tm^{3+}/$NaYF_4$ core–shell NPs have five distinct emission peaks that are located at 345 nm ($^1I_6$ → $^3F_4$), 363 nm ($^1D_2$ → $^3H_6$), 451 nm ($^1D_2$ → $^3F_4$), 477 nm ($^1G_4$ → $^3H_6$) and 644 nm ($^3F_3$ → $^3H_6$). B in Fig. 4(a) is the upconversion luminescence spectra of $NaYF_4$:Yb^{3+},Tm^{3+}/$NaYF_4$@MnO_2 composite NPs. It can be seen $NaYF_4$:Yb^{3+},Tm^{3+}/$NaYF_4$@MnO_2 composite NPs have hardly emission peaks. To facilitate the observation of the emission peaks of the composite NPs, B in Fig. 4(a) was multiplied by 40 times, resulting in C in Fig. 4(a).[28] Under 980 nm continuous pump light excitation, we can see the composite NPs have two emission peaks that are located at 477 nm ($^1G_4$ → $^3H_6$) and 644 nm ($^3F_3$ → $^3H_6$). The above phenomenon is due to the resonance energy transfer between Tm^{3+} ions and MnO_2 nanosheets,[28] which can quench the upconversion luminescence of the core–shell NPs. The mechanism diagram of the energy transfer between Tm^{3+} ions and MnO_2 nanosheets is shown in Fig. 4(b). Luminescence process of Yb^{3+}-Tm^{3+} co-doped system mainly consists of excited state absorption (ESA), energy transfer upconversion (ETU) and cross-relaxation (CR). For the up-conversion luminescence of the core–shell NPs, Yb^{3+} ions as sensitizers have a large absorption cross section at 980 nm. Under 980 nm continuous pump excitation, Yb^{3+} ions absorb energy to continuously transfer electrons from $^7F_{7/2}$ ground state level to $^7F_{5/2}$ excited state level, and then transfer energy to adjacent Tm^{3+} ions, so that the electrons can be populated to the excited state levels of Tm^{3+} ions, such as $^3H_5$ level, $^3F_2$ level, $^3F_3$ level and $^1G_4$ level. The energy transfer process is the following: $^2F_{5/2}$ (Yb^{3+}) + $^3F_4$ (Tm^{3+}) → $^2F_{7/2}$ (Yb^{3+}) + $^3H_5$ (Tm^{3+}), $^2F_{5/2}$ (Yb^{3+}) + $^3H_4$ (Tm^{3+}) → $^2F_{7/2}$ (Yb^{3+}) + $^3F_{2,3}$ (Tm^{3+}), $^2F_{5/2}$(Yb^{3+}) + $^3H_6$ (Tm^{3+}) → $^2F_{7/2}$ (Yb^{3+}) + $^1G_4$ (Tm^{3+}). Due to the large energy mismatch (∼3500 cm^{-1}) between Yb^{3+} ions and Tm^{3+} ions, the ions cannot be directly placed on the $^1D_2$ level of Tm^{3+} ions through energy transmission, so we need CR ($^2F_{2,3}$ (Tm^{3+}) + $^3H_4$ (Tm^{3+}) → $^1D_2$ (Tm^{3+})

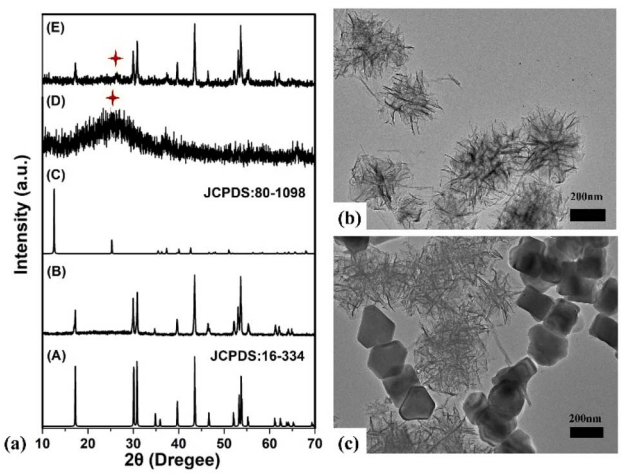

Fig. 3 (a) XRD patterns of (A) β-phase $NaYF_4$ standard card (JCPDS: 16-334), (B) $NaYF_4$:Yb^{3+},Tm^{3+}/$NaYF_4$ core–shell NPs, (C) δ-phase MnO_2 standard card (JCPDS: 80-1098), (D) MnO_2 nanosheets, (E) $NaYF_4$:Yb^{3+},Tm^{3+}/$NaYF_4$@MnO_2 composite NPs. (b) The TEM images of MnO_2 nanosheets. (c) The TEM images of $NaYF_4$:Yb^{3+},Tm^{3+}/$NaYF_4$@MnO_2 composite NPs.

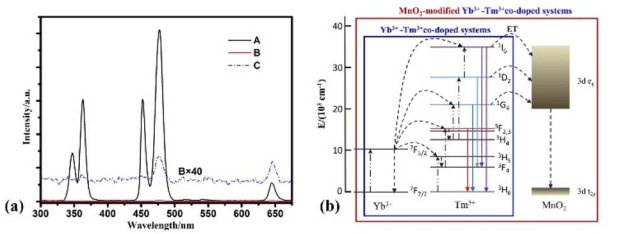

Fig. 4 (a) Upconversion spectra of (A) $NaYF_4$:18%Yb^{3+},0.5%Tm^{3+}/$NaYF_4$ core–shell NPs and (B) $NaYF_4$:18%Yb^{3+},0.5%Tm^{3+}/$NaYF_4$@MnO_2 composite NPs under 980 nm continuous pump light excitation, (C) is 40 times the product of (B). (b) The schematic diagram of the energy transfer process of Yb^{3+}-Tm^{3+} co-doped system and MnO_2-modified Yb^{3+}-Tm^{3+} codoped system under 980 nm continuous pump light excitation.[28]

+ $^3H_6$ (Tm^{3+})) process. Because of the efficient generation of CR process, more and more Tm^{3+} ions are located at the $^1D_2$ level, resulting in an effective energy transfer process of $^2F_{5/2}$ (Yb^{3+}) + $^1I_6$ (Tm^{3+}) → $^2F_{7/2}$ (Yb^{3+}) + $^3H_4$ (Tm^{3+}). Finally, Tm^{3+} ions are successfully positioned on $^3H_5$ level, $^3F_{2,3}$ level, $^1G_4$ level, $^1D_2$ level and $^1I_6$ level, and upconversion of luminescence occurs through the radiation transition.

There is a resonate energy transfer occurring between the core–shell NPs and MnO_2 nanosheets.[28] The main levels ($^3H_5$, $^3F_{2,3}$, $^1G_4$, $^1D_2$ and $^1I_6$) of Tm^{3+} ions don't produce a radiative transition, but transfer energy to the 3d e_g level of the adjacent MnO_2 nanosheets. Subsequently, the energy at the 3d e_g level of the MnO_2 nanosheets jumps by radiation transition to the 3d t_{2g} level of the MnO_2 nanosheets, thus quenching the upconversion luminescence of the core–shell NPs.

In previous studies, we found that MnO_2 nanosheets can quench the upconversion luminescence of $NaYF_4$:Yb^{3+},Tm^{3+}/$NaYF_4$ core–shell NPs. Next, we prepared an aqueous solution of 1 mL $NaYF_4$:Yb^{3+},Tm^{3+}/$NaYF_4$@MnO_2 composite NPs containing 0.008 mmol $NaYF_4$:Yb^{3+},Tm^{3+}/$NaYF_4$ core–shell NPs and 0.012 mmol MnO_2 nanosheets. To observe the changes in the upconversion luminescence properties of AA to composite NPs, we tested the upconversion luminescence spectra of $NaYF_4$:Yb^{3+},Tm^{3+}/$NaYF_4$@MnO_2 composite NPs solutions after adding different amounts of AA under 980 nm continuous pump light excitation, as shown in Fig. 5(a). Fig. 5(b) showed the intensity ratio of the emission peaks of the composite particle solutions after adding different amounts of AA at 363 nm, 477 nm, and 644 nm. Firstly, we made up an aqueous AA solution of 0.1 mmol mL^{-1}, and dropped it into a 1 mL of $NaYF_4$:Yb^{3+},Tm^{3+}/$NaYF_4$@MnO_2 composite NPs solutions, droplet amount were 0 μl, 20 μl, 40 μl, 60 μl, 80 μl, 100 μl, 120 μl and 140 μl. We see that under 980 nm continuous pump light excitation, when the droplet amount of AA aqueous solution is 0 μl (No drip of the aqueous AA solution was added), the emission peak of composite NPs is almost invisible, due to the resonance energy transfer of MnO_2 and Tm^{3+} ions, quenching the upconversion of Tm^{3+} ions. When we gradually added AA aqueous solution of 0.1 mmol mL^{-1} to the composite nanoparticle solution, we found that the upconversion luminescence of $NaYF_4$:Yb^{3+},Tm^{3+}/$NaYF_4$ core–shell NPs was gradually restored with the increasing amount of AA droplets. When the amount of AA droplets was from 20 μl to 120 μl, the upconversion luminescence intensity of Tm^{3+} ions gradually increased with the amount of aqueous AA solution. The upconversion luminescence intensity of Tm^{3+} ions is maximum when the AA droplet volume is 120 μl. When the AA droplet amount is 140 μl, the upconversion luminescence intensity of Tm^{3+} ions was almost unchanged compared with the AA drop amount of 120 μl (trend diagram of changes of luminescence intensity is shown in Fig. 5(b)). From the above results, it is known that when the droplet amount of AA solution is 120 μl, it completely reacts with MnO_2 in the composite particles, that is, 0.012 mmol AA just completely reacts with 0.012 mmol MnO_2. This is because MnO_2 can be effectively deoxidize to Mn^{2+} ions by AA, meanwhile AA is oxidized to DAA. The specific reaction process is as follows[29]

$$MnO_2 + AA + 8H^+ \rightarrow Mn^{2+} + DAA + 4H_2O \quad (1)$$

Resonance energy transfer can't occur between Mn^{2+} ions and Tm^{3+} ions, so when the MnO_2 in the composite particles completely reacts with AA, the upconversion luminescence of core–shell NPs is restored. Fig. 5(a) also demonstrated that AA can restore the upconversion fluorescence of $NaYF_4$:Yb^{3+},Tm^{3+}/$NaYF_4$ core–shell NPs, without changing the position of emission peaks of the upconversion luminescence of the core–shell NPs.

We have previously proved that MnO_2 can quench the upconversion luminescence of $NaYF_4$:Yb^{3+},Tm^{3+}/$NaYF_4$ core–shell NPs and AA can deoxidize MnO_2 to Mn^{2+} ions to restore the upconversion luminescence of $NaYF_4$:Yb^{3+},Tm^{3+}/$NaYF_4$ core–shell NPs. Next, we used $NaYF_4$:Yb^{3+},Tm^{3+}/$NaYF_4$@MnO_2 composite NPs as anti-counterfeiting materials to conduct experiments on anti-counterfeiting research. We used the prepared $NaYF_4$:Yb^{3+},Tm^{3+}/$NaYF_4$@MnO_2 composite NPs aqueous solution as anti-counterfeiting materials to write the letter "L" on the paper. Under natural light environment, we can see the black letter "L" on the paper, the photograph was shown in Fig. 5(c). There was no change about letter "L" under 980 nm continuous pump light irradiation, the photograph was shown in Fig. 5(d). After smearing AA aqueous solution, the black of letter "L" disappeared, the photograph was shown in Fig. 5(e). At this point, letter "L" emitted bright blue-purple fluorescence under 980 nm continuous pump light irradiation, the photograph was shown in Fig. 5(f). Therefore, the $NaYF_4$:Yb^{3+},Tm^{3+}/$NaYF_4$@MnO_2 composite NPs can be applied in the field of fluorescence anti-counterfeiting, and composite NPs need to deoxidize by specific reducing agents to display fluorescence

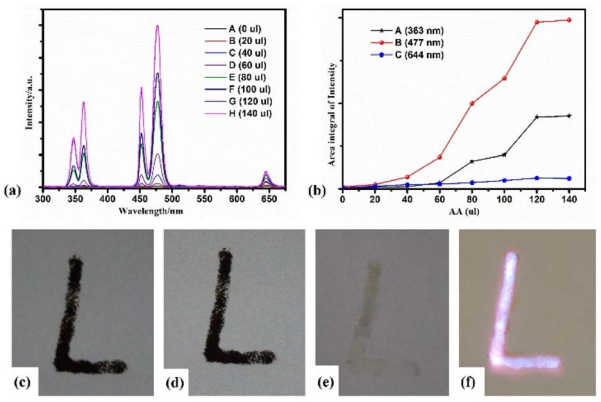

Fig. 5 (a) Upconversion luminescence spectra of $NaYF_4$:Yb^{3+},Tm^{3+}/$NaYF_4$@MnO_2 composite NPs solutions after adding different amounts of AA (b) the intensity ratio of the emission peaks of $NaYF_4$:Yb^{3+},Tm^{3+}/$NaYF_4$@MnO_2 composite NPs solutions after adding different amounts of AA at 363 nm, 477 nm, and 644 nm. The droplet amount of AA of 0.1 mmol mL^{-1} drops is A–H: 0–140 μl. (c) Photograph of the letter "L" written by $NaYF_4$:Yb^{3+},Tm^{3+}/$NaYF_4$@MnO_2 composite NPs aqueous solution. (d) Photograph of (c) under 980 nm continuous pump light irradiation. (e) Photograph of the letter "L" after smearing AA aqueous solution. (f) Photograph of (e) under 980 nm continuous pump light irradiation.

under continuous pump light irradiation, which is more safe than ordinary fluorescence anti-counterfeiting.

To test the stability of $NaYF_4$:Yb^{3+},Tm^{3+}/$NaYF_4$@MnO_2 composite NPs, three identical samples of $NaYF_4$:Yb^{3+},Tm^{3+}/$NaYF_4$@MnO_2 composite NPs were synthesized. On the first day, the fluorescence spectra of the three samples were tested under 980 nm continuous light excitation, as shown in Fig. 6(a) at 1, 2, and 3. On the 10th day, the fluorescence spectra of the three samples were obtained under 98 0 nm continuous light excitation, as shown in Fig. 6(a) at 4, 5, and 6. On the 60th day, the fluorescence spectra of the three samples were measured under 980 nm continuous light excitation, as shown in Fig. 6(a) at 7, 8, and 9. Then, these three samples were reduced by AA and the fluorescence properties of the three samples after adding AA were tested. On the first day, the fluorescence spectra of the three samples after adding AA were tested under 980 nm continuous light excitation, as shown in 1, 2, and 3 of Fig. 6(b). On the 10th day, the fluorescence spectra of the three samples after adding AA were obtained under 980 nm continuous light excitation, as shown in 4, 5, and 6 of Fig. 6(b). On the 60th day, the fluorescence spectra of the three samples after adding AA were measured under 980 nm continuous light excitation, as shown in 7, 8, and 9 of Fig. 6(b). Fig. 6(c) show comparison of the luminescence intensity of $NaYF_4$:Yb^{3+},Tm^{3+}/$NaYF_4$@MnO_2 composite NPs at 477.6 nm under continuous pump light excitation at 980 nm. The results indicate that $NaYF_4$:Yb^{3+},Tm^{3+}/$NaYF_4$@MnO_2 composite NPs exhibit reliable fluorescence characteristics and good experimental reproducibility, under the excitation of 980 nm continuous light. Fig. 6(d) show comparison of the luminescence intensity of $NaYF_4$:Yb^{3+},Tm^{3+}/$NaYF_4$@MnO_2 composite NPs after adding AA at 477.6 nm under continuous pump light excitation at 980 nm. From Fig. 6(d), it can be seen that $NaYF_4$:Yb^{3+},Tm^{3+}/$NaYF_4$@MnO_2 composite NPs after adding AA exhibit reliable fluorescence characteristics and good experimental reproducibility, under the excitation of 980 nm continuous light. Fig. 6(e) show under 980 nm continuous pump light excitation, the luminescence intensity of the three $NaYF_4$:Yb^{3+},Tm^{3+}/$NaYF_4$@MnO_2 composite NPs samples at 477.6 nm was measured on the 1st, 10th, and 60th day, respectively. From Fig. 6(e), it can be seen that $NaYF_4$:Yb^{3+},Tm^{3+}/$NaYF_4$@MnO_2 composite NPs has good stability. Fig. 6(f) show under 980 nm continuous pump light excitation, the luminescence intensity of the three $NaYF_4$:Yb^{3+},Tm^{3+}/$NaYF_4$@MnO_2 composite NPs samples after adding AA at 477.6 nm was measured on the 1st, 10th, and 60th day, respectively. Fig. 6(f) shows that $NaYF_4$:Yb^{3+},Tm^{3+}/$NaYF_4$@MnO_2 composite NPs s after adding AA has also good stability."

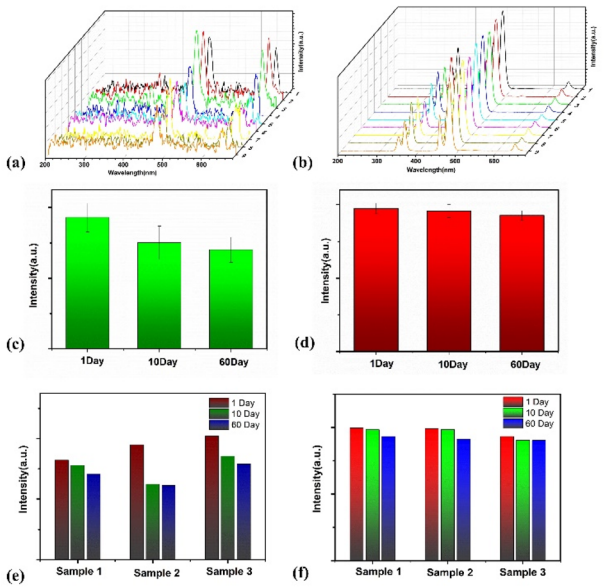

Fig. 6 (a) Upconversion spectra of $NaYF_4$:Yb^{3+},Tm^{3+}/$NaYF_4$@MnO_2 composite NPs under 980 nm continuous pump light excitation. (b) Upconversion luminescence spectra of $NaYF_4$:Yb^{3+},Tm^{3+}/$NaYF_4$@MnO_2 composite NPs after adding AA. (c) Comparison of the luminescence intensity of $NaYF_4$:Yb^{3+},Tm^{3+}/$NaYF_4$@MnO_2 composite NPs at 477.6 nm under continuous pump light excitation at 980 nm. (d) Comparison of the luminescence intensity of $NaYF_4$:Yb^{3+},Tm^{3+}/$NaYF_4$@MnO_2 composite NPs after adding AA at 477.6 nm under continuous pump light excitation at 980 nm. (e) Under 980 nm continuous pump light excitation, the luminescence intensity of the three samples at 477.6 nm was measured on the 1st, 10th, and 60th day, respectively. (f) Under 980 nm continuous pump light excitation, the luminescence intensity of the three samples after adding AA at 477.6 nm was measured on the 1st, 10th, and 60th day, respectively.

4. Conclusion

In summary, we presented a method to improve the upconversion luminescence intensity of $NaYF_4$:18%Yb^{3+},0.5%Tm^{3+} core NPs, that is, a $NaYF_4$ passive shell was wrapped outside the core NPs. Compared with $NaYF_4$:18%Yb^{3+},0.5%Tm^{3+} core NPs, the upconversion luminescence intensity (~477 nm) of $NaYF_4$:18%Yb^{3+},0.5%Tm^{3+}/$NaYF_4$ core–shell NPs was increased by 2.3 times. We also reported a novel design based on composite particles of physical mixing of rare-earth upconversion NPs and MnO_2 nanosheets, which can further enhance the security of fluorescence anti-counterfeiting. In this design, MnO_2 nanosheets can be used as a quencher for the upconversion luminescence of rare earth ions. The AA can destroy the structure of MnO_2 and reduce it to Mn^{2+} ions, which can't conduct resonant energy transfer with rare earth ions, so the upconversion luminescence of rare earth ions restore. Rare earth materials after using a specific reducing agent can display fluorescence under pump light to make fluorescence security more encryption.

Data availability

The authors confirm that the data supporting the findings of this study are available within the article.

Author contributions

Y. Z. and X. L. conceived and designed the experiments; Y. Z. and X. L. performed the experiments; Y. Z., Y. W. M. S. and Z. Q. analyzed the data and contributed reagents/materials/analysis tools. Y. Z. and X. L. wrote the paper. All authors have read and agreed to the published version of the manuscript.

Conflicts of interest

There are no conflicts to declare.

Acknowledgements

This research was funded by the Jilin Provincial Natural Science Foundation No. YDZJ202201ZYTS425. Jilin Institute of Chemical Technology Doctoral Initiation Fund Project, No. 2023011. TEM data was obtained using equipment maintained by Jilin Insititute of Chemical Technology Center of Characterization and Analysis.

References

1 W. J. Yao, Q. Y. Tian and W. Wu, *Adv. Opt. Mater.*, 2018, **7**, 1801171; A. Abdollahi, H. Roghani-Mamaqani, B. Razavi and M. Salami-Kalajahi, *ACS Nano*, 2020, **14**, 14417–14492.
2 L. Yan, H. Zheng, Q. Zhang, B. Zhou, L. Yan, J. Huang, Z. An, Q. Zhang and B. Zhou, *Nano Lett.*, 2022, **22**, 7042–7048.
3 Y. Wu, X. Chen and W. Wu, *Small*, 2023, **19**, 2206709.
4 J. M. Meruga, W. M. Cross, P. S. May, Q. Luu, G. A. Crawford and J. J. Kellar, *Nanotechnology*, 2012, **23**, 395201.
5 P. Kumar, J. Dwivedi and B. K. Gupta, *J. Mater. Chem. C*, 2014, **2**, 10468–10475.
6 K. Park, M. Park, H. S. Jang, J. H. Park, J. Kim, Y. Cho, I. K. Han, D. J. Byun and H. Ko, *Adv. Funct. Mater.*, 2018, **28**, 1800369.
7 T. Y. Sun, B. Z. Xu, B. Chen, X. Chen, M. Y. Li, P. Shi and F. Wang, *Nanoscale*, 2017, **9**, 2701–2705.
8 L. G. Zhang, S. L. Zhao, Z. Q. Liang, J. J. Zhang, W. Zhu, P. Liu and H. K. Sun, *J. Alloys Compd.*, 2017, **699**, 1–6.
9 L. Anbharasi, M. Gunaseelan, V. N. K. B. Adusumalli, S. Yamini, V. Mahalingam and J. Senthilselvan, *AIP Conf. Proc.*, 2019, **2115**, 030179.
10 F. Auzel, *Chem. Rev.*, 2004, **104**, 139–173.
11 M. Nyk, R. Kumar, T. Y. Ohulchanskyy, E. J. Bergey and P. N. Prasad, *Nano Lett.*, 2008, **8**, 3834–3838.
12 B. Marco, C. Luís and X. G. Liu, *Phys. Today*, 2015, **68**, 38–44.
13 M. Haase and H. Schäfer, *Angew. Chem., Int. Ed.*, 2011, **50**, 5808–5829.
14 X. Chen, D. F. Peng, Q. Ju and F. Wang, *Chem. Soc. Rev.*, 2015, **44**, 1318–1330.
15 B. Zhou, B. Y. Shi, D. Y. Jin and X. G. Liu, *Nat. Nanotechnol.*, 2015, **10**, 924–936.
16 L. Lei, D. Q. Chen, C. Li, F. Huang, J. J. Zhang and S. Q. Xu, *J. Mater. Chem. C*, 2018, **6**, 5427–5433.
17 Q. Q. Ma, J. Wang, Z. H. Li, D. Wang, X. X. Hu, Y. S. Xu and Q. Yuan, *Inorg. Chem. Front.*, 2017, **4**, 1166–1172.
18 Y. L. Liu, K. L. Ai and L. H. Lu, *Nanoscale*, 2011, **3**, 4804–4810.
19 M. L. You, J. J. Zhong, Y. Hong, Z. F. Duan, M. Lin and F. Xu, *Nanoscale*, 2015, **7**, 4423–4431.
20 M. X. Li, W. J. Yao, J. Liu, Q. Y. Tian, L. Liu, J. Ding, Q. W. Xue, Q. Lu and W. Wu, *J. Mater. Chem. C*, 2017, **5**, 6512–6520.
21 W. J. Yao, Q. Y. Tian, J. Liu, Z. H. Wu, S. Y. Cui, J. Ding, Z. G. Dai and W. Wu, *J. Mater. Chem. C*, 2016, **4**, 6327–6335.
22 Y. D. Han, H. Y. Li, Y. B. Wang, Y. Pan, L. Huang, F. Song and W. Huang, *Sci. Rep.*, 2017, **7**, 1320.
23 Y. L. Zhang, P. Lv, X. Liu, H. Y. Chi, G. Q. Xi and Z. K. Qin, *Nano*, 2020, **15**, 2050023–2050031.
24 Y. L. Zhang, X. H. Liu, Y. B. Lang, Z. Yuan, D. Zhao, G. S. Qin and W. P. Qin, *J. Mater. Chem. C*, 2015, **3**, 2045–2053.
25 Y. L. Zhang, F. Wang, Y. B Lang, J. Yin, M. L. Zhang, X. H. Liu, D. M. Zhang, D. Zhao, G. S. Qin and W. P. Qin, *J. Mater. Chem.*, 2015, **3**, 9827–9832.
26 Y. Zhang, S. J. Deng, Y. H. Li, B. Liu, G. X. Pan, Q. Liu, X. L. Wang, X. H. Xia and J. P. Tu, *Energy Stor. Mater.*, 2020, **29**, 52–59.
27 D. Q. Chen and P. Huang, *Dalton Trans.*, 2014, **43**, 11299–11304.
28 R. R. Deng, X. J. Xie, M. Vendrell, Y. T. Chang and X. G. Liu, *J. Am. Chem. Soc.*, 2011, **133**, 20168–20171.
29 Q. Yang, X. Y. Wang, H. L. Peng, M. Arabi, J. H. Li, H. Xiong, J. Choo and L. G. Chen, *Sens. Actuators, B*, 2019, **302**, 127176.